

Towards a resolution of the proton form factor problem: new electron and positron scattering data

D. Adikaram,^{1,*} D. Rimal,^{2,†} L.B. Weinstein,^{1,‡} B. Raue,² P. Khetarpal,² R.P. Bennett,¹ J. Arrington,³ and W.K. Brooks⁴

(The CLAS Collaboration)

¹*Old Dominion University, Norfolk, Virginia 23529*

²*Florida International University, Miami, Florida 33199*

³*Argonne National Laboratory, Argonne, Illinois 60441*

⁴*Universidad Técnica Federico Santa María, Casilla 110-V Valparaíso, Chile*

(Dated: November 24, 2014)

There is a significant discrepancy between the values of the proton electric form factor, G_E^p , extracted using unpolarized and polarized electron scattering. Calculations predict that small two-photon exchange (TPE) contributions can significantly affect the extraction of G_E^p from the unpolarized electron-proton cross sections. We determined the TPE contribution by measuring the ratio of positron-proton to electron-proton elastic scattering cross sections using a , simultaneous, tertiary electron-positron beam incident on a liquid hydrogen target and detecting the scattered particles in the Jefferson Lab CLAS detector. This novel technique allowed us to cover a wide range in virtual photon polarization (ε) and momentum transfer (Q^2) simultaneously, as well as to cancel luminosity-related systematic errors. The cross section ratio increases with decreasing ε at $Q^2 = 1.45 \text{ GeV}^2$. This measurement is consistent with the size of the form factor discrepancy at $Q^2 \approx 1.75 \text{ GeV}^2$ and with hadronic calculations including nucleon and Δ intermediate states, which have been shown to resolve the discrepancy up to $2 - 3 \text{ GeV}^2$.

PACS numbers: 14.20.Dh,13.60.Fz,13.40.Gp

The electromagnetic form factors describe fundamental aspects of nucleon structure. However, measurements of the ratio of the electric to magnetic proton form factors, $\mu_p G_E(Q^2)/G_M(Q^2)$, (μ_p is the proton anomalous magnetic moment) extracted using unpolarized and polarized electron elastic scattering data differ by a factor of three at momentum transfer squared $Q^2 \approx 6 \text{ GeV}^2$ [1–9]. Until the cause of this surprising discrepancy is fully understood, the uncertainty in the form factors can affect the determination of the proton radius, the interpretation of color transparency and ($e, e'p$) proton knockout measurements, comparisons to isovector and isoscalar nucleon structure calculations from Lattice QCD [10], and measurements to extract the flavor-dependent quark contributions to the form factors from parity-violating asymmetries [11].

One possible explanation for the discrepancy is the presence of two-photon exchange (TPE) effects, where the electron exchanges a virtual photon with the proton, possibly exciting it to a higher state, and then exchanges a second virtual photon, de-exciting the proton back to its ground state. TPE effects are suppressed by an additional power of the fine structure constant $\alpha = e^2/\hbar \approx 1/137$ [12–16]. Calculations indicate that TPE effects are small, but increase with electron scattering angle [17, 18]. Because unpolarized measurements of the charge form factor, G_E , extract it from the angular dependence of the elastic cross section at fixed momentum transfer, and because the G_E -dependent part of the cross-section is small compared to the G_M -dependent

part at large Q^2 , even the small angle-dependent TPE correction can lead to large corrections to $\mu_p G_E/G_M$. However, calculation of the TPE contributions requires a knowledge of *all* the baryonic resonance and continuum states that can couple to the two virtual photons. These corrections are therefore not yet sufficiently well understood to be applied to the data and are typically neglected in calculating radiative corrections [19–21].

The most direct way to measure the TPE contributions to the cross section is by measuring the ratio of positron-proton to electron-proton elastic scattering. However, due to the low luminosity of secondary positron beams, existing measurements of the e^+p/e^-p cross section ratio are statistically limited and unable to constrain the TPE contribution [22–25]. Two new experiments, VEPP-3 at Novosibirsk and OLYMPUS at DESY, will measure the e^+p and e^-p cross sections sequentially using electron and positron beams in storage rings [26–28].

In this work, we used a unique technique to compare e^+p and e^-p scattering. Rather than alternating between mono-energetic e^+ and e^- beams, we generated a combined electron-positron beam covering a range of energies and detected the scattered lepton and struck proton in the CEBAF Large Acceptance Spectrometer (CLAS) at the Thomas Jefferson National Accelerator Facility (Jefferson Lab). This let us simultaneously cover a wide range of momentum transfers and virtual photon polarization, $\varepsilon = [1 + 2(1 + \tau) \tan^2(\theta/2)]^{-1}$, where $\tau = \frac{Q^2}{4M_p^2}$. By measuring the e^+p and e^-p elastic cross sections simultaneously, luminosity-related systematic uncertain-

ties cancelled. This paper briefly describes the lepton beam line, the analysis techniques, and the results of the CLAS TPE experiment.

The lepton-proton elastic scattering cross section is proportional to the square of the sum of the Born amplitude and all higher-order QED correction amplitudes. The ratio of $e^\pm p$ elastic scattering cross sections can be written as [29]:

$$R = \frac{\sigma(e^+p)}{\sigma(e^-p)} \approx \frac{1 + \delta_{even} - \delta_{2\gamma} - \delta_{brem}}{1 + \delta_{even} + \delta_{2\gamma} + \delta_{brem}} \approx 1 - 2(\delta_{2\gamma} + \delta_{brem})/(1 + \delta_{even}), \quad (1)$$

where δ_{even} is the total charge-even radiative correction factor, and $\delta_{2\gamma}$ and δ_{brem} are the fractional TPE and lepton-proton bremsstrahlung interference contributions. The second line is valid when the δ_i terms are small. After calculating and correcting for the charge-odd δ_{brem} term, the corrected cross section ratio is:

$$R' \approx 1 - \frac{2\delta_{2\gamma}}{(1 + \delta_{even})}. \quad (2)$$

We produced a simultaneous tertiary beam of electrons and positrons by using the primary electron beam to produce photons and then used the photons to produce e^+e^- pairs. A 110 – 140 nA 5.5 GeV electron beam struck a 9×10^{-3} radiation length (RL) gold foil to produce a bremsstrahlung photon beam. The electrons were diverted by the Hall-B tagger magnet [30] into the tagger beam dump. The photon beam passed through a 12.7-mm diameter collimator and then struck a 9×10^{-2} RL gold foil to produce e^+e^- pairs. The combined photon-lepton beam then entered a three-dipole magnet chicane to horizontally separate the electron, positron and photon beams. The photon beam was stopped by a tungsten block in the middle of the second dipole. The lepton beams were recombined into a single beam by the third dipole and then proceeded to a 30-cm long liquid hydrogen target at the center of CLAS. For more information on the beam line, see Ref. [29]. The scattered leptons and protons were detected in the CLAS spectrometer [31].

CLAS is a nearly 4π detector. The magnetic field is provided by six superconducting coils that produce an approximately toroidal field in the azimuthal direction around the beam axis. The sectors between the six magnet cryostats are instrumented with identical detector packages. We used the three regions of drift chambers (DC) [32] to measure charged particle trajectories, scintillation counters (SC) [33] to measure time-of-flight (TOF) and forward ($\theta < 45^\circ$) electromagnetic calorimeters (EC) [34] to trigger events. The momentum resolution $\delta p/p$ is $\sim 0.6\%$. Additionally, a Sparse Fiber Monitor (SFM), located just upstream of the target, was used to monitor the lepton beam position and stability. A remotely insertable TPE calorimeter (TPECal) located downstream of CLAS measured the energy distributions

of the individual lepton beams at lower intensity before and after each chicane field reversal. A compact mini-torus magnet placed close to the target shielded the DC from Møller electrons. The CLAS event trigger required at least minimum ionizing energy deposited in the EC in any sector and a hit in the SC in the opposite sector.

In order to reduce the systematic uncertainties due to potential detector acceptance and incident beam differences, the torus magnet and beam chicane magnet currents were periodically reversed during the run period. The final data set was grouped into four magnet cycles and each magnet cycle contained all possible configurations ($c+t+$, $c+t-$, $c-t+$, $c-t-$ where c and t are the chicane and torus magnet polarities, respectively).

The symmetric production of e^+/e^- pairs gives confidence that reversing the chicane magnet polarity ensures that the ‘left beam’ luminosity for particles passing on the left side of the chicane is the same for positive-chicane positrons as for negative-chicane electrons. This in turn allows us to use the powerful ‘ratio of ratios’ technique.

The ratio between the number of e^+p and e^-p elastic scattering events is calculated in three steps. First, the single ratios are calculated for each magnet configuration as $R_1^{c\pm t\pm} = \frac{N_{e^+p}^{c\pm t\pm}}{N_{e^-p}^{c\pm t\pm}}$. Here $N_{e^\pm p}^{c\pm t\pm}$ are the number of detected elastic events for the different chicane (c) and torus (t) polarities. The proton detection acceptance and efficiency effects cancel in the single ratio. Next, the double ratios are calculated for each chicane polarity as $R_2^{c\pm} = \sqrt{R_1^{c\pm t+} R_1^{c\pm t-}}$. Any differences in proton and lepton acceptances cancel out in the double ratio. Last, the quadruple ratio is calculated as $R = \sqrt{R_2^{c+} R_2^{c-}}$. The differences in the incident e^- and e^+ beam luminosities cancel out in the quadruple ratio. The remaining effects due to lepton-proton correlations and due to the non-reversed magnetic field of the mini-torus were simulated and corrected for as described below. See Ref. [29] for details.

We applied a series of corrections and cuts to the experimental data to select the elastic $e^\pm p$ events. The systematic deviations in the reconstructed momenta and angles were studied and corrected. Fiducial cuts in angle and momentum were used to select the region of CLAS with uniform acceptance for both lepton polarities, thus matching the acceptances for electron and positron. Contamination from target entrance and exit windows was removed by a 28-cm vertex cut centered on the target on both leptons and protons.

We calculated the incident lepton energy from the measured scattering angles assuming elastic scattering as $E_l = M_p(\cot(\theta_l/2) \cot \theta_p - 1)$. Since elastic lepton-proton scattering is kinematically overdetermined when both particles are detected, we applied kinematic cuts on four quantities to select elastic events: the azimuthal angle difference between the lepton and proton ($\Delta\phi$),

the difference between the incident lepton energy (ΔE_l) calculated in two different ways, the difference between the measured and the calculated scattered lepton energy ($\Delta E'_l$) and the difference between the measured and the calculated recoiling proton momentum (Δp_p):

$$\begin{aligned}\Delta\phi &= \phi_l - \phi_p \\ \Delta E_l &= E_l - (p_l \cos\theta_l + p_p \cos\theta_p) \\ \Delta E'_l &= \frac{M_p E_l}{E_l(1 - \cos\theta_l) + M_p} - E'_l \\ \Delta p_p &= \frac{p_l \sin\theta_l}{\sin\theta_p} - p_p,\end{aligned}$$

where (p_l, θ_l, ϕ_l) and (p_p, θ_p, ϕ_p) are the measured momenta, scattering angles and azimuthal angles of the lepton and proton, respectively. The measured scattered lepton energy is $E'_l = p_l$. ΔE_l and $\Delta E'_l$ are strongly correlated so we applied cuts to $\Delta E^\pm = \Delta E_l \pm \Delta E'_l$. We identified positrons and protons kinematically. When this was ambiguous (i.e., when an event with two positive particles passed all four kinematic cuts as either e^+p or pe^+) then TOF information was used to identify the positron and proton. We applied $\pm 3\sigma$ Q^2 - and ε -dependent kinematic cuts to select elastic scattering events. The resulting spectra are remarkably clean (see Fig. 1).

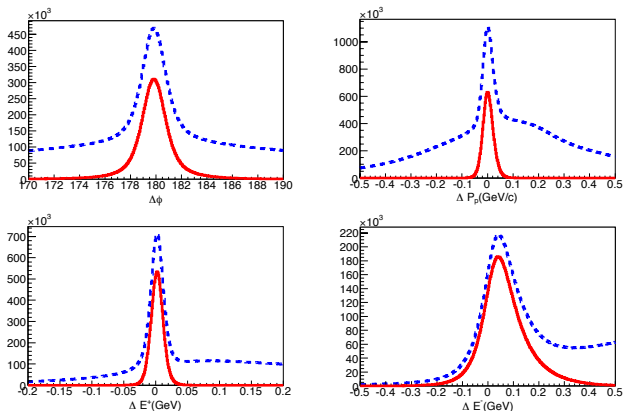


FIG. 1: (Color online) Number of events as a function of the four variables, $\Delta\phi$, ΔP_p and ΔE^\pm , before (blue dashed) and after (red) applying the other three elastic cuts on each and summed over all kinematics.

There is a remnant background seen under the signal, primarily at low ε and high Q^2 , even after all other cuts. Since this background is symmetric in $\Delta\phi$, it was estimated by fitting a Gaussian to the tails of the $\Delta\phi$ distribution. We validated the Gaussian shape of the background by comparing it to the background shape determined by the events in the tails of the ΔE^- distribution. The background was subtracted from the signal before constructing the final cross section ratio.

Malfunctioning SC channels were identified. For each $e^\pm p$ event, we simulated the passage of an identical, oppositely-charged lepton through CLAS and removed the event if either the original particles or the oppositely-charged lepton hit a malfunctioning channel.

The incident e^+ and e^- energies for both chicane polarities were reconstructed using the scattering angles of the detected e^\pm and p . The energy distribution rises rapidly from about 0.5 GeV to a peak at about 0.85 GeV and then decreases. We required $E_{incident} \geq 0.85$ GeV to avoid the region where the distribution is changing rapidly. The distributions were slightly different in shape and magnitude ($\approx 10\%$) for different beam chicane polarities, indicating that the chicane was not quite symmetric. This result is consistent with the incident lepton energy distributions as measured by the TPECAL. The TPECAL data showed that the e^+ energy distribution for positive chicane polarity was identical to the e^- energy distribution for negative chicane polarity (and vice versa). Therefore differences in e^+ and e^- beam luminosities cancel in the final ratio.

We matched the detector acceptances by selecting the region of the detector that had a uniform acceptance for both electrons and positrons (fiducial cuts) and by eliminating events that hit a dead channel or would have hit a dead channel if the lepton charge were reversed. To account for the remaining effects due to the non-reversed magnetic field of the mini-torus, we simulated events using GSIM, the CLAS GEANT-based Monte Carlo program. The resulting acceptance correction factors are all within 0.5% of unity and were applied to the measured cross section ratios.

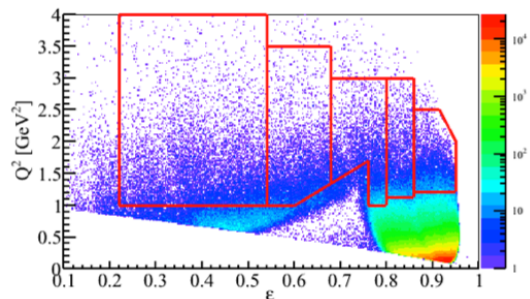


FIG. 2: (Color online) The number of e^+p elastic scattering events plotted versus Q^2 and ε for positive torus polarity. The red lines indicate the bin boundaries for the $Q^2 \approx 1.45$ GeV² data. The hole at $\varepsilon \approx 0.7$ is due to the trigger requirement that at least one of the two particles hit the EC. The holes for other configurations (negative torus polarity or e^-p events) are smaller.

Our TPE data covered a wide Q^2 - ε range (see Fig. 2). Small scattering angles θ correspond to virtual photon polarization $\varepsilon \approx 1$ and large scattering angles correspond to small ε . The $Q^2 > 1$ GeV² data were binned into five

bins in ε at an average $Q^2 = 1.45 \text{ GeV}^2$. Similarly, the $\varepsilon > 0.8$ data were binned into six Q^2 bins at an average $\varepsilon = 0.88$. The cross section ratio R was measured for each bin. It was then divided by a radiative correction factor equal to the ratio of the e^+p and e^-p radiatively corrected cross sections calculated in the modified peaking approximation [21] and averaged over each bin by Monte Carlo integration. The radiative correction ranged from 0.4% at $Q^2 = 0.23 \text{ GeV}^2$ and $\varepsilon = 0.88$ to a maximum of 3% at $Q^2 = 1.45 \text{ GeV}^2$ and $\varepsilon = 0.4$. The uncorrected, R , and radiatively corrected, R' , e^+p/e^-p cross section ratios are tabulated in the supplemental information.

Systematic uncertainties on the final ratios were carefully investigated. The uncertainty due to the target vertex cuts is the difference in the cross section ratios, R , between 26 cm and 28 cm target cuts. The uncertainty due to the fiducial cuts is the difference in R between nominal and tighter fiducial cuts. The uncertainty due to the elastic event selection is the difference in R between 3σ and 3.5σ kinematic cuts. Relaxing the elastic event selection cuts from 3σ to 3.5σ doubled the background. Thus the kinematic cut uncertainty also includes the background subtraction uncertainty. We varied the background fitting region to determine the additional uncertainty associated with the fitting procedure. We used the six-fold symmetry of CLAS to calculate R independently for each kinematic bin for leptons detected in each of the CLAS sectors (for bins and sectors with good overall efficiency). We compared the variance of the measurements with the statistically expected variance to determine the uncertainty due to detector imperfections (0.35%). The variation in R among the beam chicane magnet cycles was included as an uncertainty (0.3%). The uncertainty in the radiative correction was estimated to be 15% of the correction. The uncertainties are tabulated in the supplemental information.

Figure 3 shows the ratio R' at $Q^2 = 1.45 \text{ GeV}^2$ and at $\varepsilon = 0.88$. The calculations shown were done by Blunden *et al.* [17] and Zhou and Yang [35]. Blunden *et al.* calculated the TPE amplitude using only the elastic nucleon intermediate state. Zhou and Yang considered both the nucleon and the $\Delta(1232)$ in the intermediate state. These calculations bring the form factor ratio extracted from Rosenbluth separation measurements into good agreement with the polarization transfer measurements at $Q^2 < 2 - 3 \text{ GeV}^2$ [15].

The cross section ratio shows a moderate ε -dependence at $Q^2 = 1.45 \text{ GeV}^2$ and a slight Q^2 -dependence at $\varepsilon = 0.88$. Our data points plus the previous $\varepsilon = 0$ point [36] prefer the hadronic TPE calculation Ref. [17] by 2.5σ over the no-TPE ($R' = 0$) hypothesis. A calculation of TPE effects on a structureless point proton is disfavored by almost 5σ . Our results are consistent with the theoretical calculations and are more precise than the previous world's measurements.

We corrected the CLAS TPE cross section ratios at

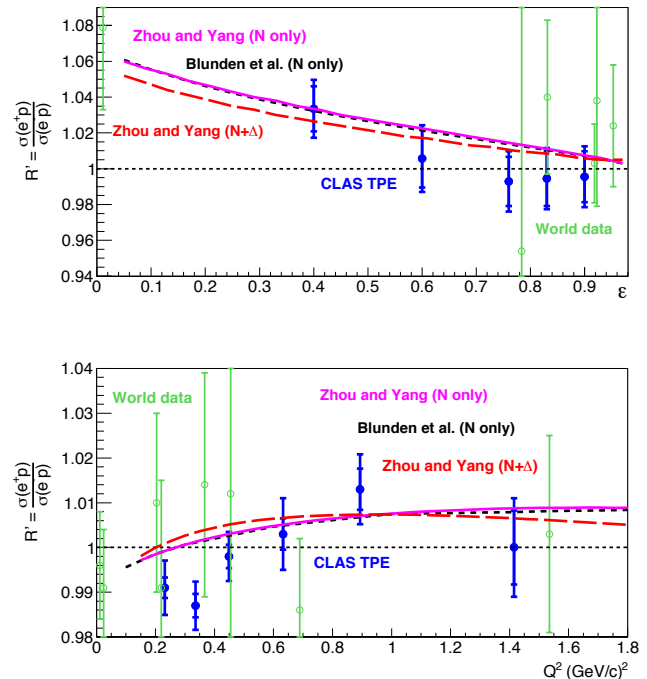


FIG. 3: (Color online) Ratio of e^+p/e^-p cross sections corrected for δ_{brem} as a function of ε at $Q^2 = 1.45 \text{ GeV}^2$ (top) and as a function of Q^2 at $\varepsilon = 0.88$ (bottom). The filled blue circles show the results of this measurement. The inner error bars are the statistical uncertainties and the outer error bars are the statistical, systematic and radiative-correction uncertainties added in quadrature. The black dotted curve shows the calculation by Blunden *et al.* [17] considering only the N intermediate state. The magenta solid and red dashed curves show the calculation by Zhou and Yang [35] including N only and $N + \Delta$ intermediate states, respectively. The open green circles show the previous world data (at $Q^2 > 1 \text{ GeV}^2$ for the top plot) [37].

$Q^2 = 1.45 \text{ GeV}^2$ for the charge-even radiative correction (see Eq. 2) averaged over the appropriate kinematic bins to determine the correction factor $1 + \delta_{2\gamma}$. We fit this to a linear function of ε and applied this as a correction factor to the reduced electron scattering cross section measurements at $Q^2 = 1.75 \text{ GeV}^2$ by Andivahis *et al.* [1]:

$$\sigma_R^{corr}(\varepsilon) = \sigma_R(\varepsilon) (1 + \delta_{2\gamma}(\varepsilon)). \quad (3)$$

Fig. 4 shows the original reduced cross section measurements from Andivahis *et al.* [1] and the CLAS TPE corrected values as a function of ε . The slope and intercept of the linear fits to the data give $G_E^2/\tau G_D^2$ and G_M^2/G_D^2 , respectively. The TPE corrections change the proton form factor ratio obtained from the unpolarized data from $\mu_p G_E/G_M = 0.910 \pm 0.060$ to 0.816 ± 0.076 , bringing it into good agreement with the polarized electron scattering result of 0.789 ± 0.042 [7]. This can be seen graphically in Fig. 4 where the slope of the ‘Unpo-

larized + TPE' cross section is much closer to that of the polarized results.

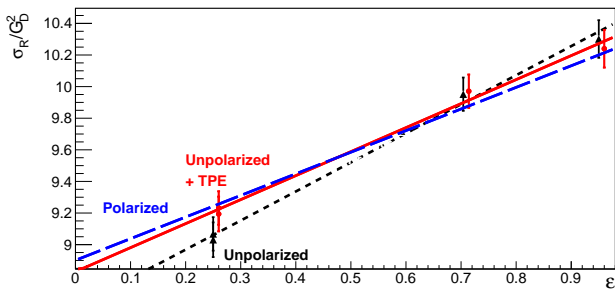


FIG. 4: (Color online) Reduced cross sections divided by the square of the dipole form factor, $G_D^2 = \left(1 + \frac{Q^2}{0.71 \text{ GeV}^2}\right)^2$, plotted as a function of ε . The black triangles show the original unpolarized measurements from Andivahis *et al.* [1] and the red circles show those cross sections corrected by the measured $\delta_{2\gamma}$. The dotted black and solid red lines show the corresponding linear fits where the slope is proportional to G_E^2 and the intercept is proportional to G_M^2 . The dashed blue line shows the slope expected from the polarized measurement of Punjabi *et al.* [7] (the intercept of this line is arbitrary).

In conclusion, we have measured the ratio of e^+p/e^-p elastic scattering cross sections over a wide range of Q^2 and ε using an innovative simultaneous tertiary e^+e^- beam, detecting the scattered particles in the CLAS spectrometer. The results are much more precise than previous measurements. At $Q^2 = 1.45 \text{ GeV}^2$, the e^+p/e^-p cross section ratio increases moderately with decreasing ε , consistent with theoretical calculations which bring the form factor ratio extracted from unpolarized electron scattering (Rosenbluth separation) measurements into good agreement with the polarized electron scattering measurements at $Q^2 < 2 - 3 \text{ GeV}^2$ [15]. The TPE corrections determined by this experiment significantly decrease the form factor ratio measured by unpolarized elastic scattering data at $Q^2 \sim 1.75 \text{ GeV}^2$ and bring it into good agreement with that determined from polarized measurements. However, the theoretical TPE calculations do not fully resolve the discrepancy at higher Q^2 [15, 35]. High Q^2 [28] and low Q^2 [38] measurements for electrons and muons will further map out the size of TPE effects and examine their impact on the proton radius and other topics.

We acknowledge the outstanding efforts of the Jefferson Lab staff (especially Dave Kashy and the CLAS technical staff) that made this experiment possible. This work was supported in part by the U.S. Department of Energy and National Science Foundation, the Italian Istituto Nazionale di Fisica Nucleare, the Chilean Comisión Nacional de Investigación Científica y Tecnológica (CONICYT), the French Centre National de la Recherche Scientifique and Commissariat à l'Energie Atomique, the

UK Science and Technology Facilities Council (STFC), and the National Research Foundation of Korea. Jefferson Science Associates, LLC, operates the Thomas Jefferson National Accelerator Facility for the United States Department of Energy under contract DE-AC05-06OR23177.

* Current address: Thomas Jefferson National Accelerator Facility, Newport News, VA 23606

† Current address: University of Florida, Gainesville, FL 32611

‡ Contact Author weinstein@odu.edu

- [1] L. Andivahis *et al.*, Phys. Rev. D **50**, 5491 (1994).
- [2] M. K. Jones *et al.*, Phys. Rev. Lett. **84**, 1398 (2000).
- [3] O. Gayou *et al.*, Phys. Rev. Lett. **88**, 092301 (2002).
- [4] J. Arrington, Phys. Rev. C **68**, 034325 (2003).
- [5] M. E. Christy *et al.*, Phys. Rev. C **70**, 015206 (2004).
- [6] I. A. Qattan *et al.*, Phys. Rev. Lett. **94**, 142301 (2005).
- [7] V. Punjabi *et al.*, Phys. Rev. C **71**, 055202 (2005).
- [8] A. J. R. Puckett *et al.*, Phys. Rev. Lett. **104**, 242301 (2010).
- [9] A. J. R. Puckett *et al.*, Phys. Rev. C **85**, 045203 (2012).
- [10] C. Alexandrou, G. Koutsou, J. W. Negele, and A. Tsapalis, Phys. Rev. D **74**, 034508 (2006).
- [11] D. H. Beck, Phys. Rev. **D39**, 3248 (1989).
- [12] P. A. M. Guichon and M. Vanderhaeghen, Phys. Rev. Lett. **91**, 142303 (2003).
- [13] P. G. Blunden, W. Melnitchouk, and J. A. Tjon, Phys. Rev. Lett. **91**, 142304 (2003).
- [14] J. Arrington, Phys. Rev. C **71**, 015202 (2005).
- [15] J. Arrington *et al.*, Prog. Part. Nucl. Phys. **66**, 782 (2011).
- [16] C. E. Carlson and M. Vanderhaeghen, Ann. Rev. Nucl. Part. Sci. **57**, 171 (2007).
- [17] P. G. Blunden *et al.*, Phys. Rev. C **72**, 034612 (2005).
- [18] A. V. Afanasev and C. E. Carlson, Phys. Rev. Lett. **94**, 212301 (2005).
- [19] L. W. Mo and Y.-S. Tsai, Rev. Mod. Phys. **41**, 205 (1969).
- [20] Y. S. Tsai, Tech. Rep., SLAC-PUB-848 (1971).
- [21] R. Ent *et al.*, Phys. Rev. **C64**, 054610 (2001).
- [22] J. Mar *et al.*, Phys. Rev. Lett. **21**, 482 (1968).
- [23] R. L. Anderson *et al.*, Phys. Rev. **166**, 1336 (1968).
- [24] W. Bartel *et al.*, Phys. Rev. Lett. **17**, 608 (1966).
- [25] J. Arrington, Phys. Rev. C **69**, 032201 (2004).
- [26] A. Gramolin *et al.*, Nucl. Phys. Proc. Suppl. **225-227**, 216 (2012).
- [27] J. Arrington *et al.* (2004), arXiv:nucl-ex/0408020.
- [28] R. Milner *et al.*, Nucl. Inst. Meth. A **741**, 1 (2014).
- [29] M. Moteabbed *et al.* (CLAS Collaboration), Phys. Rev. C **88**, 025210 (2013).
- [30] D. I. Sober *et al.*, Nucl. Instr. Methods A **440**, 263 (2000).
- [31] B. A. Mecking *et al.*, Nucl. Instr. Methods A **503**, 513 (2003).
- [32] M. D. Mestayer *et al.*, Nucl. Instr. Methods A **449**, 81 (2000).
- [33] E. S. Smith *et al.*, Nucl. Instr. Methods A **432**, 265 (1999).
- [34] M. Amarian *et al.*, Nucl. Instr. Methods A **460**, 239

- (2001).
- [35] H.-Q. Zhou and S. N. Yang (2014), 1407.2711.
- [36] B. Bouquet, D. Benaksas, B. Grossetete, B. Jean-Marie, G. Parrou, J. P. Poux, and R. Tchapoutian, Phys. Lett. **B26**, 178 (1968).
- [37] J. Arrington, Phys. Rev. C **69**, 032201 (2004), URL <http://link.aps.org/doi/10.1103/PhysRevC.69.032201>.
- [38] R. Gilman et al. (MUSE Collaboration) (2013), arXiv:1303.2160.